International Journal of Science and Research (IJSR)
ISSN (Online): 2319-7064
Index Copernicus Value (2013): 6.14 | Impact Factor (2013): 4.438

Synergetic Visible Light Degradation of Methyl Orange, Rhodamine B and Methylene Blue Over Supra Stoichiometric Ferric and Bismuth Molybdates

P. Suresh*, T. Narasimha Murthy, A. V. Prasada Rao

Andhra University

*E-mail:sureshp12345@gmail.com

Abstract: ***$Fe_2(MoO_4)_3$ and $Bi_2(MoO_4)_3$ have been prepared by solution mixing and glycene combustion methods using Bi/Fe nitrate, ammonium heptamolybdate/molybdic acid as precursors. The heat treated precursor powders were characterized in terms of TG, DTA, XRD and FTIR. Phase pure samples were obtained at 400°C with combustion method. Suprastoichiometric samples consisting of excess MoO_3 showed enhanced photocatalytic activity for the degradation of Rhodamine B, Methylene blue and Methyl orange dyes in presence of H_2O_2 under visible light irradiation. Rates of photo degradation observed with Fe/Bi-Molybdate $xMoO_3$ were higher than those obtained for Degusa P25 under the same experimental conditions.***

Keywords: $Fe_2(MoO_4)_3$; $Bi_2(MoO_4)_3$; Rhodamine B; Methylene Blue; Methyl orange; Photo degradation

1. Introduction

Ever since the projection of TiO_2 as a potential photo catalyst for remediation of organic dye pollutants in waste water effluents from textile, dye, ink, cosmetic and food industries, various strategies have been explored either to shift the absorption edge of TiO_2 from U.V to visible region or to enhance its photo catalytic activity by other means. The different scientific approaches in this regard comprise of (i) doping TiO_2 with metal atoms, anions and/or cations (Zaleska, 2008) (ii) coating TiO_2 with photo sensitizers such as metal pthalocyanins or metal phorphyrins or dyes to exploit higher absorption by sensitizer with subsequent charge transfer from sensitizer to host material (Guptha and Manoj, 2011) and (iii) formation of hetero nanostructures of mesoporus or hierarchical or hallow composites with materials of suitable band potential (Rajeshwar et al., 2001). Though, doping with certain anions or cations have been found to shift the absorption of TiO_2 into visible region, the process is limited by low efficiency because the induced dopant energy levels also serve as sites for electron-hole recombination and tend to lower the photo catalytic activity. Dye sensitization proved to be more useful in photo splitting of H_2O than photocatalysis. Similarly, formation of nano structures is limited to model studies and may not be cost effective for industrial applications. Consequently, several attempts have been contemplated to develop alternate non-TiO_2 based materials which can exhibit good photo catalytic activity by absorbing large part of solar radiation. A few of the potentially projected newly developed mixed metal oxide semiconductors reported with visible light photocatalytic activity include Bi_2MoO_6 (Ji-Mei et al., 2013), $Bi_2Mo_3O_{12}$ (Suresh and Prasada Rao, 2015), $Fe_2Mo_3O_{12}$ (Suresh et al., 2014) and Bi_2WO_6 (Zhou and Zhu, 2012).

Among the various ternary metal oxide photo catalysts, metal molybdates form a seperate class of functional materials because of their useful applications in photoluminescence, optical fibers, scintillation materials, humidity sensors and catalysis. It is also well established in catalytic industry that supra stoichiometric Bi and Fe-molybdates exhibit higher catalytic activities compared to respective stoichiometric Bi/Fe-molybdates (Beale et al., 2009; Graselli, 1997). The enhanced catalytic activity has been attributed to contact synergy, remote control, and co-operative phenomenon, ferric ion deficiency caused by substitution of $Mo^{(VI)}$ in place of $Fe^{(III)}$, formation of MoO_3 layer on active catalyst surface and to higher selectivity of MoO_3 phase (Soares et al., 2001a; 2003b, 2004c; Soderhjelm et al., 2008; Routray et al., 2010; Soares et al., 2015). But, to our knowledge, no reports exist in literature as to whether a similar synergetic or cooperative effect that was evident in conventional catalysis also exists between MoO_3 and Fe/Bi-molybdate photocatalysts as MoO_3 is also an n-type semiconductor with a wide band gap. Since only stoichiometric Bi/Fe-molybdates have been investigated as photocatalysts for degradation of hardly a couple of dyes (Tian et al., 2011; De la Cruz et al., 2010) the present work is therefore taken up to investigate whether any synergetic effect is also operative in H_2O_2 assisted visible light photo degradation of Rhodamine-B, Methylene blue and Methyl orange over supra stoichiometric $M_2(MoO_4)_3$ $xMoO_3$ where M=Bi, Fe.

2. Materials and Methods

All solutions were prepared in doubly distilled water. All the chemicals used in this study were of analytical grade. $Fe(NO_3)_3$, D-Manitol were obtained from sigma-Aldrich India Ltd. $Bi(NO_3)_3$ (99%), Glycene (99.7%), $NaHCO_3$ and NaCl were obtained from Merck India Ltd. Ammonium heptamolybdate was obtained from BDH, Poland. H_2MoO_4 (85% as MoO3) and MoO_3 (99.5%) were obtained from Loba Chimie, India.

$Fe_2Mo_3O_{12}$ and $Bi_2Mo_3O_{12}$ were synthesized by two different methods using two different precursors- ammonium heptamolybdate and molybdic acid for Mo.

(i) Solution Mixing Method:

Stoichiometric quantities of $Fe(NO_3)_3$ and H_2MoO_4/Ammonium heptamolybdates are separately dissolved in minimum amount of 1:1 HNO_3 and the solutions are mixed together under constant stirring and pH 2.0 is maintained by adding 0.1 N Ammonia and stirred for 5 hr at 40-50^oC. The resultant cloudy solution was evaporated at 80^oC, and the powder was calcined at 400^oC for 4 hr. The calcined powder was ground and used for phase identification and photo catalytic study. The precursor powders obtained using ammonium heptamolybdate and H_2MoO_4 are hereafter referred to as sample 1 and sample 2 respectively.

(ii) Combustion Method:

$Fe(NO_3)_3.5H_2O$/$Bi(NO_3)_3$, Ammoniumheptamolybdate and H_2MoO_4 of AR Quality were starting materials. Stoichiometric amounts of metal nitrates and Mo-precursors were added to 50 ml of water under constant stirring followed by the addition of suitable amount of glycine. The mixture was then heated on a hot plate at 110℃ under constant stirring until it became viscous with liberation of large amounts of brown fumes. The dried mass was then calcined at 400℃ for 4 hr and resultant Ferric and Bismuth samples are hereafter referred to as sample 3 and sample 4. The same procedure is adopted for the synthesis of stoichiometric $M_2(MoO_4)_3$ and supra stoichiometric $M_2(MoO_4)_3$ $xMoO_3$ where M=Bi or Fe using MoO_3 as precursor for Mo.

Characterization

Phase purity of dried gel powders heat treated at different temperatures and resultant powder from combustion were investigated with X-ray diffractometer (PANalytical- X' Pert PRO, Japan) at room temperature, using Nickel filtered Cu-K_α radiation (λ= 1.54059 Å), with a scan rate of 2° min^{-1}. FT-IR data for precursors as well as heat treated precursors have been obtained with schimadzu IR prestige - 21.

Photo Catalytic Studies

Photo catalytic activity of $Bi_2(MoO_4)_3$ was evaluated in terms of degradation of Methyl orange (MO), Rhodamine B (Rh-B) and Methylene blue (MB) under visible light irradiation using 400W metal halide lamp as light source for irradiation. UV radiation below 350nm is eliminated by surrounding the sample with a water jacket. 100 mg of the catalyst powder was added into 100ml dye aqueous solution (10 mg/L) and the suspension was magnetically stirred for half an hour in dark and the suspension was then exposed to light emanating from the source; 5ml aliquots of the dye aqueous solutions were pipetted at periodic time intervals and filtered through 0.45 micron Millipore filters to remove the suspended particles. Progress of decolorization was assessed in terms of the corresponding absorption spectra. All the experiments were conducted under ambient conditions. Degradation of dye is calculated by the following equation

% degradation of dye = A_0-A/A_0*100

Where A_0 and A are respectively initial absorbance and absorbance at time 't' of the dye.

Photoluminescence Studies:

50mg suprastoichiometric $Bi_2Mo_3O_{12}$/ $Fe_2Mo_3O_{12}$ catalyst is added to 100ml of terpthalic acid (TPA) solution (0.25 mmol L^{-1} in 1mmol L^{-1} NaOH solution). The solution is stirred for 30min in dark followed by irradiation by 400w metal halide lamp for 30min and 45min. The reacted solution was centrifuged and the clear solution is used for photoluminescence measurements in a fluorescence spectro flourometer (Flouromax 4) with the excitation wavelength of 315nm.

3. Results and Discussion

Thermogravimetric (TG) and Differential Thermal Analysis (DTA)

Thermogravimetric (TG) and Differential thermal analysis (DTA) behaviour of dried precursor powders obtained from $Fe(NO_3)_3$ with ammonium heptamolybdatae (sample 1), $Fe(NO_3)_3$ with H_2MoO_4 (sample 2), final product after combustion of ferric nitrate and MoO_3 with glycene (sample 3) and Bismuth molybdate precursor powder (sample 4) are shown in Fig 1. Thermogram of sample 1 (Fig 1(a)) showed a continuous weight loss from 50^oC to 280 ^oC followed by a plateau from 280^oC to 800^oC. Thermogram of sample 2 also showed a weight loss from 150-280^oC followed by a plateau from 300-800^oC (Fig 1(a)). Difference in initial temperature for weight loss of sample 1 and sample 2 must be due to variation in gel drying times. The observed weight loss in sample 1 is ascribed to evolution of NO, NH_3 and H_2O whereas in sample 2 the weight loss may be due to NO and H_2O due to decomposition of the respective precursors. Thermograms of sample 3 and 4 did not show any weight loss and this is expected because the mixed solution containing glycene is already heated at 150^oC for 5 hr (Fig 1 (b)). DTA curves of samples 1 and 2 showed small endothermic peaks below 200^oC followed by one broad endothermic peak in the temperature region of 200-300^oC and a sharp endothermic peak at 650^oC. The appearance of small endothermic peaks were previously reported for $Bi_2(MoO_4)_3$ synthesis from $Bi(NO_3)_3$ and ammonium molybdate by several investigators who attributed them to rearrangement of H-bonds in molybdate (De la Cruz et al., 2009). Since the temperature of second broad endothermic peak in both cases coincides with the weight loss region in respective TG curves, the peak is assigned to decomposition of precursors. The sharp endothermic peak at 650 ^oC, which occurs in the corresponding plateau regions of respective TG curves, may arise due to either a phase transition or melting. Since $Fe_2(MoO_4)_3$ was reported to melt congruently at 940-975^oC the endothermic peak is ascribed to a phase transformation of $Fe_2(MoO_4)_3$ from monoclinic to orthorhombic structure based on observed colour change of

sample to yellowish green and XRD data matching with orthorhombic $Fe_2(MoO_4)_3$ discussed later. DTA curves of samples 3 and 4 also show sharp endothermic peaks around the same temperature. These are ascribed to phase transition in $Fe_2(MoO_4)_3$ and melting in $Bi_2(MoO_4)_3$ samples respectively. Since no crystallization peak is present in the DTA curves of samples 1 and 2, the precursor powders were heat treated at 400°C for 4 hr and heat treated samples were investigated by XRD for phase identification.

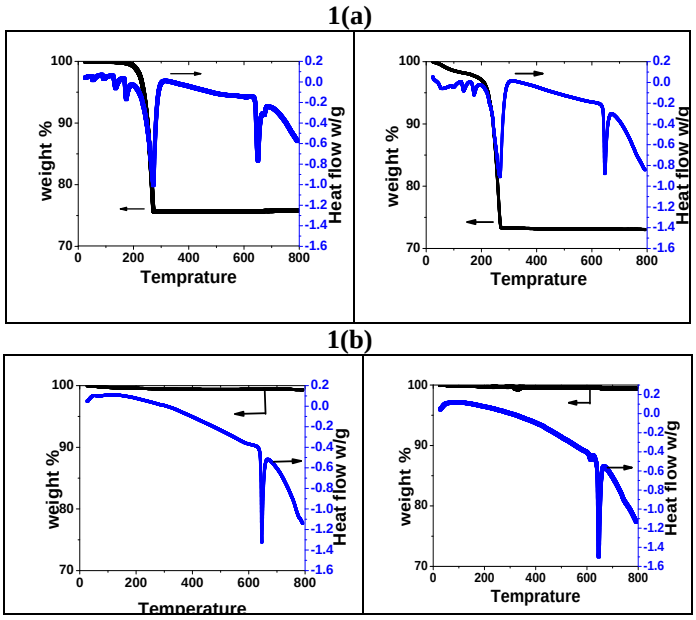

Figure 1 (a): TG and DTA curves for dried precursor powders obtained from mixed solutions of $Fe(NO_3)_3$ with ammoniumhepta molybdate/ H_2MoO_4, **(b)** TG and DTA curves for resulting powders obtained after solution combustion for mixture of glycine with Fe/Bi- nitrate and H_2MoO_4

X-Ray Diffraction Study

XRD patterns of samples 1, 2, 3 and 4 heat treated at 400°C are shown in (Fig 2). XRD pattern of sample 1 heat treated at 400°C for 4 hr shows emergence of peaks due to formation of $Fe_2Mo_3O_{12}$. Intensities of these peaks increased when the sample is heat treated at 500°C for 4 hr. All of peaks in the XRD pattern could be indexed to monoclinic $Fe_2(MoO_4)_3$ of JCPDS file N0 72-0935. XRD pattern of sample 1 heat treated at 800°C for 4 hr showed peaks characteristic of orthorhombic $Fe_2(MoO_4)_3$ (JCPDS File No 80-0195). XRD pattern of sample 2 heat treated at 500°C did not show peaks characteristic of $Fe_2Mo_3O_{12}$ indicating that sample 2 requires still higher heat treatment temperature for complete phase formation of $Fe_2(MoO_4)_3$. XRD patterns of Samples 3 and 4 corresponding to heat treatment at 400°C for 4 hr showed sharp diffraction peaks all of which could be indexed to mono phasic $Fe_2(MoO_4)_3$ irrespective of Mo-precursor.

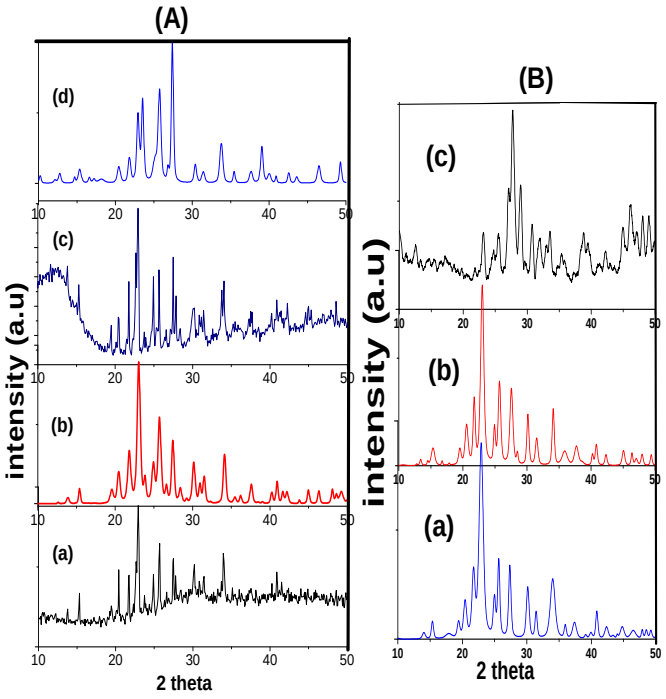

Figure 2: (A) XRD patterns of dried precursor powders obtained from sample (1) heat treated at (a) 400°C, (b) 500 °C, (c) 800 °C and (d) sample (2) heat treated at 500 °C.(B) XRD patterns of resulting powders from combustion synthesis at 400 °C for 4 hr of sample (3) (a) Ammonium heptamolybdate precursor, (b) H_2MoO_4 precursor and (c) sample 4 with MoO_3.

FTIR Study

Room temperature precursors and heat treated precursor powders are further characterized by FTIR spectroscopy. Fig 3 depicts the FTIR spectra of room temperature precursors obtained for sample 1 and 2 (Fig 3a and 3b) heat treated at 500°C for 4 hr respectively (Fig 3c and 3d) and for samples 3 and 4 heat treated at 400°C for 4 hr (Fig 3e and 3f). From the FTIR spectra of these samples it is clear that complete formation of phase pure $Fe_2Mo_3O_{12}$ is seen only in the case of samples obtained from combustion synthesis. Broad band between 700 cm^{-1} to 950 cm^{-1} in Fig 3(e) is ascribed to the stretching vibrations of Mo-O bonds in non-equivalent tetrahedral positions. Band at 593cm^{-1} corresponds to stretching vibrations of octahedral six coordinated Mo species in $Fe_2Mo_3O_{12}$. Narrow peaks observed around at 960 and 999cm^{-1} are attributed to Fe-O-Mo and Mo=O stretching vibrations respectively. The FTIR spectrum shown in Fig 3(e) is in complete agreement with earlier reports for $Fe_2Mo_3O_{12}$ (Singh et al., 2009; Soares, 2001). Similarly FTIR spectrum shown in Fig 3(f) agrees well with the literature reports for $Bi_2Mo_3O_{12}$ (Zhao et al., 2009; Gizybowska et al., 1972) All the observed absorption bands are accounted for in terms of Mo-O stretching bands and deformation modes involving Bi-O vibrations. From the above results, it is seen that combustion synthesis yielded phase pure Bi/Fe-molybdates at temperatures as low as 400°C. Hence, the solution combustion method has been adopted for the synthesis of stoichiometric and suprastoichiometric Fe/Bi-molybdates for photo degradation studies.

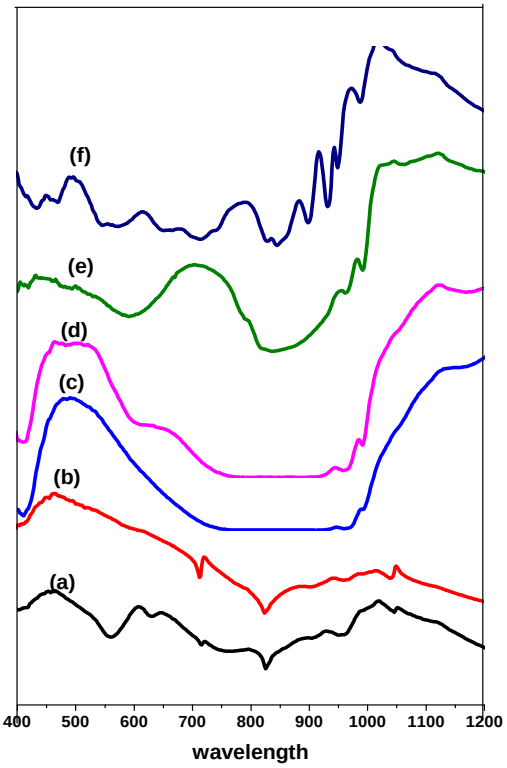

Figure 3: FTIR Spectra of (a) Room temperature precursor powder for sample 1, (b) precursor powder for sample 2, (c) sample (1) heat treated at 500°C for 4h, (d) sample 2 heat treated at 500°C for 4 hr, (e) resultant powder after combustion of sample (3) and (f) resultant powder after combustion of sample (4)

Photocatalytic Degradation of Dyes

Methyl orange, an azo dye is known to be toxic, mutagenic and carcinogenic. Degradation of MO has been reported with α-Fe_2O_3 (Sharma et al., 2014), Er^{3+}: $YAlO_3/TiO_2$ (Dong et al., 2014), ZnO/Zn-stannate (Danwittayakul et al., 2013) nano ZnO (Daniel Souza et al., 2013), TiO_2 (Hu et al., 2010) Ag/N-TiO_2 (Wu and Long, 2012), CuO doped ZnO (Razali et al., 2011), Phosphotungstic acid (Zhong and Jun bo, 2013), nano SnO_2 (yuan and Xu, 2010), $SrTiO_3$ (Puangpetch et al., 2006). In the above reports except for Er^{3+}: $YAlO_3/TiO_2$ and Ag/N-TiO_2 the irradiation source is U.V and photo degradation times varied from 80 to 540min. and even for those with visible light irradiation, photo degradation times were rather high (480min). Temporal variation of spectral changes as a function of irradiation time are shown in Fig 4 for aqueous methyl orange+H_2O_2 containing (a) stoichiometric $Fe_2(MoO_4)_3$ (b) $Fe_2(MoO_4)_3$ with excess MoO_3 (c) stoichiometric $Bi_2(MoO_4)_3$ (d) $Bi_2(MoO_4)_3$ with excess MoO_3 (e) no photo catalyst and (f) TiO_2 (Degusa P25). From the change in intensity as observed in Figures 4(a) and 4(b), it can be seen that stoichiometric $Fe_2(MoO_4)_3$ could affect complete degradation in 60min while $Fe_2(MoO_4)_3$+MoO_3 could complete the same degradation for 45min of irradiation. The difference in degradation time is more apparent with $Bi_2(MoO_4)_3$ (Fig 4c and 4d). Stoichiometric $Bi_2(MoO_4)_3$ could not effect complete degradation even for 240min of exposure while $Bi_2(MoO_4)_3$ with excess MoO_3 could complete the dye degradation for 120min of exposure. In the absence of either photo catalyst, degradation due to H_2O_2 is negligible as can be seen from 4e. Degussa P25 under similar conditions required 180min of exposure for 68% dye degradation.

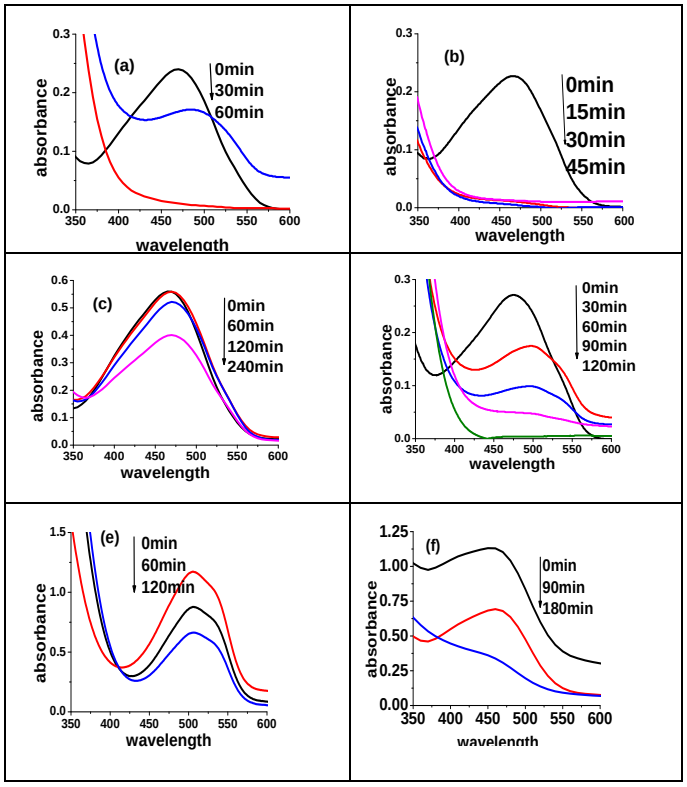

Figure 4: Temporal evolution of spectral variations as a function of exposure time for aqueous methyl orange+ H_2O_2 containing (a) stoichiometric $Fe_2(MoO_4)_3$ (b)$Fe_2(MoO_4)_3$ xMoO_3 (c) stoichiometric $Bi_2(MoO_4)_3$ (d) $Bi_2(MoO_4)_3$ xMoO_3 (e) MoO_3 (f) with Degussa P25 (TiO_2)

Rhodamine B, one of the commonly used xanthene dye is used as a colorant in textiles and food stuffs. It is harmful to both human beings and animals due to its toxicity and carcinogenicity. Photo degradation of Rhodamine B has been reported over ZnO (Hiremath et al., 2014), Pt-TiO_2 (Obuya et al., 2014), TiO_2/ZnO (Zhang, 2013), TiO_2 and ZnO (Cao et al., 2013), α-$Bi_2Mo_3O_{12}$ (de la Cruz et al., 2010). In all these cases, the reported photo degradation times varied from 130 to 360min. Change in spectral intensities as a function of irradiation time for aqueous Rh-B+H_2O_2 containing (a) $Fe_2(MoO_4)_3$, (b) $Fe_2(MoO_4)_3$ xMoO_3, (c) $Bi_2(MoO_4)_3$, (d) $Bi_2(MoO_4)_3$ xMoO_3, (e) no photo catalyst and (f) Degussa P25 are shown in Fig 5. Stoichiometric $Fe_2(MoO_4)_3$ could affect 47.2% degradation for 120min of exposure. Whereas supra stoichiometric $Fe_2(MoO_4)_3$ effected complete degradation for 50min of irradiation. Similarly, stoichiometric $Bi_2Mo_3O_{12}$ caused 100% degradation for 150min of irradiation while $Bi_2(MoO_4)_3$ with excess MoO_3 caused complete degradation for 60min of exposure (Fig 5c and 5d). In the absence of photo catalyst, degradation due to H_2O_2 is very small (Fig 5e) and with Degussa P25, the degradation occurred for 180min of exposure.

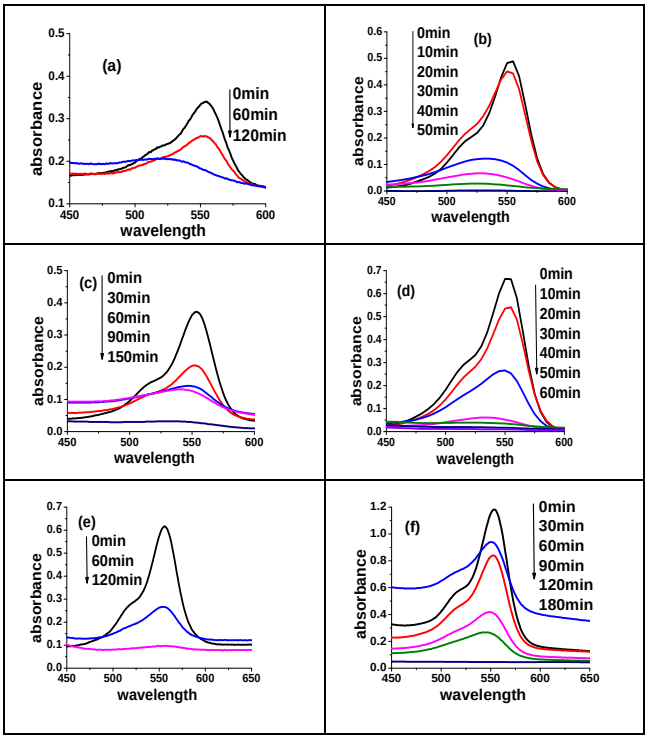

Figure 5: Temporal evolution of spectral variations as a function of exposure time for aqueous Rhodamine B+H_2O_2 containing (a) stoichometric $Fe_2(MoO_4)_3$ (b) $Fe_2(MoO_4)_3$ with excess MoO_3 (c) stoihiometric $Bi_2(MoO_4)_3$ (d) $Bi_2(MoO_4)_3$ with excess MoO_3 (e) with MoO_3 (f) with Degussa P25 (TiO_2)

Methylene blue a thiazene class of dye is also used as colorant photo degradation of methylene blue was reported with nano ZnO (Kuriakose et al., 2013), nano TiO_2 (Aliabadi and Hajiabadi, 2013), W/Mo doped TiO_2 (Akbarzadeh and Javadpour, 2014), Ag/TiO_2 (Torkian and Amereh, 2012) and the reported degradation times varied from 60 to 300min. Temporal variation of spectral changes as a function of irradiation time for aqueous solution of methylene blue+H_2O_2 containing (a) stoichiometric $Fe_2(MoO_4)_3$, (b) $Fe_2(MoO_4)_3$ with excess MoO_3, (c) stoichiometric $Bi_2(MoO_4)_3$, (d) $Bi_2(MoO_4)_3$ with excess MoO_3, (e) no photo catalyst and (f) Degusa P25 are shown in Fig 6. Stoichiometric $Fe_2(MoO_4)_3$ and $Fe_2(MoO_4)_3$ with excess MoO_3 caused complete degradation for the exposure time of 120min and 90min respectively (Fig 6a and 6b). However, stoichiometric $Bi_2(MoO_4)_3$ could affect only 58.2% degradation for 90min of exposure while $Bi_2(MoO_4)_3$ xMoO_3 caused complete degradation for 60min exposure (Fig 6c and 6d). In the absence of any photo catalyst, H_2O_2 itself caused 72% degradation for 120min exposure. Degussa P25 could degrade the MB under the same conditions for 180min of irradiation. The calculated rates of degradation obtained from ln C/C_0 vs irradiation time plots over stoichiometric and supra stoichiometric Bi/Fe-molybdate, MoO_3 and TiO_2 photocatalysts for MO, Rh-B and MB are given in Table 1.

Table 1: Rate constants for photodegradation reactions of MO, Rh-B and MB over different photocatalysts

Photocatalyst used	Degradation rate constants for		
	Methy orange	Rhodamine B	Methylene blue
$Fe_2(MoO_4)_3$	$7.1*10^{-4}$	$4.1*10^{-4}$	$1.6*10^{-4}$
$Fe_2(MoO_4)_3$ xMoO_3	$1.7*10^{-3}$	$1.6*10^{-3}$	$3.8*10^{-4}$
$Bi_2(MoO_4)_3$	$4.1*10^{-6}$	$1.0*10^{-4}$	$1.0*10^{-4}$
$Bi_2(MoO_4)_3$ xMoO_3	$2.2*10^{-4}$	$1.1*10^{-3}$	$\approx 1.0*10^{-3}$
MoO_3	$3.3*10^{-5}$	$1.3*10^{-4}$	$7.5*10^{-5}$
Degussa P25	$3.3*10^{-5}$	$8.3*10^{-5}$	$8.3*10^{-5}$

The variations in rates of degradation indicate that photocatalytic degradation mechanism is different in Bi and Fe-molybdate systems. In the case of $Bi_2(MoO_4)_3$ xMoO_3 since the band gap difference between MoO_3 (2.9 eV), and $Bi_2(MoO_4)_3$ (3.1 eV) is small, the two components exert a synergetic effect in generating more electrons in the conduction band of $Bi_2(MoO_4)_3$. As a consequence there will be an increase in $^{\cdot}OH$ free radicals as per the steps 1, 2 and 3 in the mechanism given below.

$MoO_3 + h\upsilon \rightarrow MoO_3 (e^-_{CB} + h^+_{VB})$ ----- (1)

$MoO_3 (e^-_{CB} + h^+_{VB}) + i_2(MoO_4)_3 \rightarrow Bi_2(MoO_4)_3(e^-_{CB} + h^+_{VB})$ ------(2)

$Bi_2(MoO_4)_3 + h\upsilon \rightarrow Bi_2(MoO_4)_3(e^-_{CB} + h^+_{VB})$ ------(3)

$Bi_2(MoO_4)_3(e^-_{CB}) + H_2O_2 \rightarrow {}^-OH + {}^{\cdot}OH + Bi_2(MoO_4)_3$ -----(4)

$Bi_2(MoO_4)_3(h^+_{VB}) + {}^-OH \rightarrow {}^{\cdot}OH$ -----(5)

Dye + $^{\cdot}OH \rightarrow$ degradation products ------ (6)

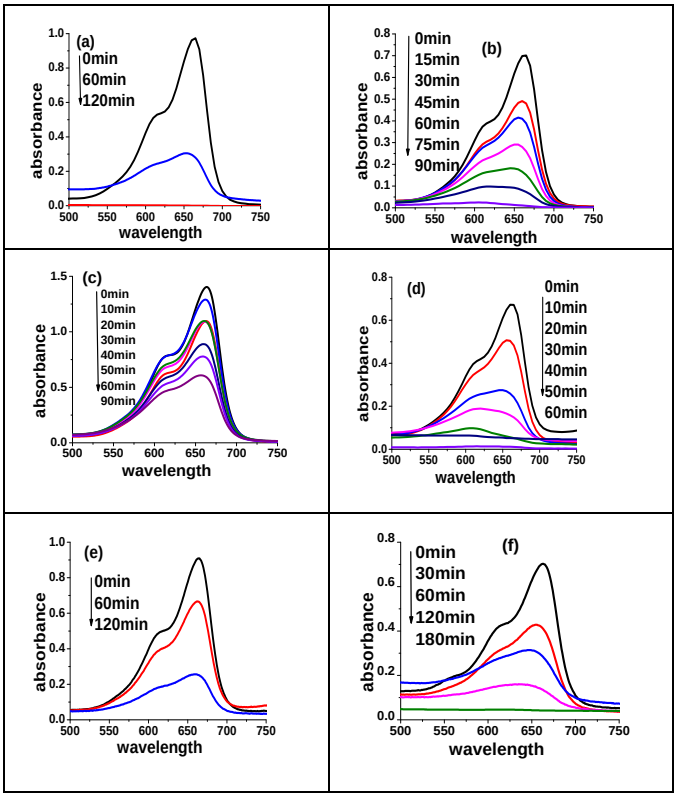

Figure 6: Temporal evolution of spectral variations as a function of exposure time for aqueous Methylene blue+H_2O_2 containing (a) stoichometric $Fe_2(MoO_4)_3$ (b)

$Fe_2(MoO_4)_3$ with excess MoO_3 (c) stoihiometric $Bi_2(MoO_4)_3$ (d) $Bi_2(MoO_4)_3$ with excess MoO_3 (e) with MoO_3 (f) with Degussa P25 (TiO_2)

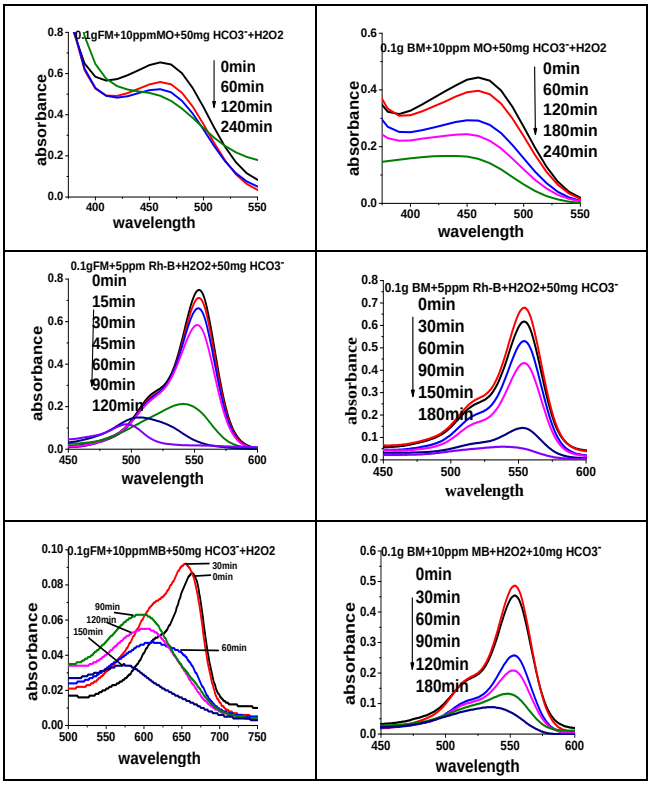

Figure 7: Effect of HCO_3^- on the degradation times for Rh-B, MB and MO over $Fe_2(MoO_4)_3$ $xMoO_3$ and $Bi_2(MoO_4)_3$ $xMoO_3$ photocatalysts

Formation of $^{\cdot}OH$ during the reaction is confirmed with the increase in degradation time due to scavenging effect of HCO_3^- as shown in Fig 7 for the three dyes over $Bi_2(MoO_4)_3$ xMoO3 and $Fe_2(MoO_4)_3$ $xMoO_3$ photocatalysts. In presence of HCO_3^- the degradation times are much higher due to removal of $^{\cdot}OH$ by HCO_3^-. However, in the case of $Fe_2(MoO_4)_3$ $xMoO_3$, the band gap difference between MoO_3 and $Fe_2(MoO_4)_3$ is not beneficial to $Fe_2(MoO_4)_3$ since E_{gap} for $Fe_2(MoO_4)_3$ is 2.2 eV where as E_{gap} for MoO_3 is 2.9 eV. In view of higher band gap of MoO_3, as compared to $Fe_2(MoO_4)_3$ there will not be any synergetic effect. However, there will be a cooperative effect due to MoO_3 but this will be much less compared to the synergy between $Bi_2(MoO_4)_3$ and MoO_3. This is evident from the variation in intensities in the photoluminescence spectra for $^{\cdot}OH$ with TPA as shown in Fig 8 for suprastoichiometric $Bi_2(MoO_4)_3$ and $Fe_2(MoO_4)_3$ systems. From the figure, it is evident that, the PL intensity due to $^{\cdot}OH$ in $Bi_2(MoO_4)_3$ $xMoO_3$ is much higher compared to PL intensity due to $^{\cdot}OH$ in $Fe_2(MoO_4)_3$ $xMoO_3$. Mechanism operative in $Fe_2(MoO_4)_3$ must therefore be in terms of other reactions like Fenton process and formation of molybdenum peroxocomplexes which are also capable of causing dye degradation.

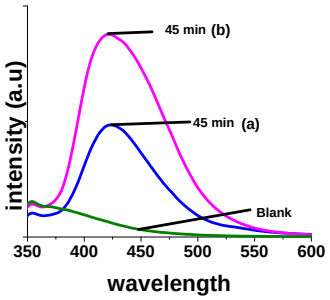

Figure 8: Photoluminescence spectra

Above experimental data clearly indicates that presence of excess MoO_3 is more beneficial with $Bi_2(MoO_4)_3$ than with $Fe_2(MoO_4)_3$ in expediting the degradation process. The data further shows that both $Fe_2(MoO_4)_3$ and $Bi_2(MoO_4)_3$ with excess MoO_3 exhibit higher rate of degradation compared to Degussa P25 under the same experimental conditions.

4. Conclusions

$M_2(MoO_4)_3$ and $M_2(MoO_4)_3$ $xMoO_3$ where M=Bi and Fe were synthesized by both solution mixing and combustion methods. The heat treated precursor powders were characterized in terms of TG, DTA, XRD and FTIR. Photocatalytic degradation studies were done for Mo, Rh-B and MB dyes over stoichiometric and suprastoichiometric Bi/Fe-molybdates. Synergetic interactions between $Bi_2(MoO_4)_3$-MoO_3 and cooperative effect between $Fe_2(MoO_4)_3$-MoO_3 were observable in dye degradation studies. Lesser degradation times were obtained over these above photocatalysts compared to TiO_2 (Degussa P25) under similar conditions.

Acknowledgment

One of the authors (P.S) is grateful to the Council of Scientific and Industrial Research, New Delhi, India for the financial support in the form of SRF.

References

[1] Aliabadi, M., Hajiabadi, M., photocatalytic degradation of Methylene blue in aqueous solutions using TiO_2 nanoparticles. 2013. J. Bio &Env. Sci. 3, 8-12.
[2] Akbarzadeh, R., Javadpour, S., 2014. W/Mo-doped TiO_2 for photocatalytic degradation of Methylene blue. Int. J. Eng. Sci. Innovative Tech. 3, 621-629.
[3] Beale, A.M., Jacques, S.D.M., Sacaliuc-Parvulescu, E., O'Brien, M.G., Barnes, P., Weckhuysen, B.M., 2009. An iron molybdate catalyst for methanol to formaldehyde conversion prepared by a hydrothermal method and its characterization. Appl. Catal. A: Gen. 363, 143-152.
[4] Daniel Souza, A.R., Gusatti, M., Sanches, C., Moser, V.M., Kuhnen, N.C., Riella, H.G., 2013. Initial studies of photocatalytic discolouration of methyl orange by using ZnO nano structures. Chem. Eng. Trans. 32, 2275-2280.
[5] Danwittayakul, S., Jaisai, M., Koottatep, T., Dutta, J., 2013. Enhancement of photocatalytic degradation of methyl orange by supported zinc oxide nanorods/zinc stannate (ZNO/ZTO) on porous substrates. Ind. Eng. Chem. Res. 52, 1369-13636.
[6] De la Cruz, A.M., Alfaro, S.O., Marcos Villarreal, S.M.G., photocatalytic behavior of α-$Bi_2Mo_3O_{12}$ prepared by the

pichini method: degradation of organic dyes under visible-light irradiation, 2010. Res. Chem. Intermed. 36, 925-936.
[7] De la Cruz, A.M., Obregon Alfaro, S., 2009. Synthesis and characterization of nanoparticles of α-$Bi_2Mo_3O_{12}$ prepared by co-precipitation method: Langmuir adsorption parameters and photocatalytic properties with rhodamine B. Solid state sciences. 11 829-835.
[8] Dong, S., Zhang, X., He, F., Dong, S., Zhou, D., Wang, B., 2015. Visible light photocatalytic degradation of methyl orange over spherical activated carbon supported and Er^{3+}: $YAlO_3$- doped TiO_2 in a fluidized bed. J. Chem. Technol. Biotechnol. 90, 880-887.
[9] Du, P., Song, L., Xiong, J., Cao, H., 2013. Photocatalytic degradation of Rhodamine B using electrospun TiO_2 and ZnO. J. Mater. Sci. 48, 8386-8392.
[10] Graselli, R.K., (1997) in hand book of heterogeneous catalysis; Ertl, G., Knozinger, H., Weitkamp, J., Eds.; VCH: Germany, 5, 2302.
[11] Gizybowska, B., Haber, J., Komorek, J., 1972. The chemistry of Bi-Mo oxide catalysts: 1. Phase composition of catalysts and its relation to the structure of precursors. J. Catal. 25, 25-32.
[12] Guptha,S.M., Manoj, T., 2011. A review of TiO_2 nanoparticles, Chinese Sci. Bull. **56,** 1639-1657.
[13] Hiremath, S., Vidya, C., Lourdu Antonyraj, M.A., Chandraprabha, M.N., Srinidhi, R., Manjunath, R., Padmanabha, Agrawal, H., 2014. Photocatalytic degradation of Rhodamine B using Bio synthesized ZnO. Int. Rev. Appl. Biotech. Biochem. 2, 207-213.
[14] Hu, Q., Liu, B., Zhang, Z., Song, M., Zhao, X., 2010. Temperature effect on the photocatalytic degradation of methyl orange under UV-vis light irradiation. J. Wuhan University Technology- Mater. Sci. Ed. 25 (2), 210 – 213.
[15] Ji- Mei, S., Hai-Qin, H., Xue- Feng, M., Ya-Li, S., Ming-Song, R., Gang, H., 2013. Surfactant-assisted hydrothermal synthesis and photocatalytic activity of octahedral γ-Bi_2MoO_6. J. Anhui University (Natural Science Edition), **37,** 73-79.
[16] Kuriakose, S., Bhardwaj, N., Singh, J., Satpati, B., Mohapatra, S., 2013. Structural, optical and photocatalytic properties of flower like ZnO nanostructures prepared by a facile wet chemical method. Beilstein J. Nanotechnol. 4, 763-770.
[17] Masteri-Farahani, M., Hosseini, H.S., 2012. Synthesis and characterization of bismuthmolybdate nanoparticles within nanoreactors of reverse micelles. Powder Technol.228, 228-230.
[18] Obuya, E.A., Joshi P.C., Gray, T.A., Keane, T.C., Jones Jr W.E., 2014. Application of Pt.TiO_2 nanofibers in photosensitized degradation of Rhodamine B. Int. J. Chem. 6, 1-16.
[19] Puangpetch, T., Sreethawongpetch, T., Chavadej, S., Yoshikawa, S., 2006. The 2nd Joint International conference on "sustainable energy and environment (SEE 2006)". Bangkok, Thailand. Nov 1-23.
[20] Rajeshwar, K., de Tacconi, N.R., Chenthamarakshan, C.R., 2001. Semiconductor based composite materials: preparation, properties and performance. Chem. Mater. 13, 2765-2782.
[21] Razali, N.Z., Halim Abdullah, A., Jelas Haron, Md., 2011. Degradation of methyl orange mediated byCuO-doped ZnO photocatalysts. Environ. Eng. Manag. J. 10, 1523-1528.
[22] Routray, K., Zhou, W., Christopher, J.K., Wolfgang, G., Israel, E.W., 2010. Origin of the synergistic interaction between MoO_3 and iron molybdate for the selective oxidation of methanol to formaldehyde. J. Catal. 275, 84-98.
[23] Soares, A.P.V., Portela, M.F., Kiennemann, A., Hilaire, L., 2003. Mechanism of deactivation of iron-molybdate catalysts prepared by coprecipitation and sol-gel techniques in methanol to formaldehyde oxidation. Chem. Eng. Sci. 58, 1315-1322
[24] Soares, A.P.V., Portela, M.F., Kiennemann, A., 2004. Methanol selective oxidation to formaldehyde over iron-molybdate catalysts. Catalysis Reviews. 47, 125-174.
[25] Soares, A.P.V., Fatima, M., Portela, M.F., Kiennemann, A., 2015. The role of the suprastoichiometric molybdenum during methanol to formaldehyde oxidation over Mo-Fe mixed oxides. Mole. Catal. A: Chem. 397, 93-98.
[26] Soares, A.P.V., Portela, M.F., Kiennemann, A., Hilaire, L., Millet, J.M.M., 2001. Iron molybdate catalysts for mrthanol to formaldehyde oxidataion: effects of Mo excess on catalytic behavior. Appl. Catal. A: Gen. 206, 221-229.
[27] Soderhjelm, E., House, M.P., Cruise, N., Holmberg, J., Bowker, M., Bovin J.O., Andersson, A., 2008. On the synergy effect in MoO_3-Fe2(MoO4)3 catalysts for methanol oxidation to formaldehyde. Top Catal. 50, 145-155.
[28] Sharma, P., Kumar, R., Chauhan, S., Singh, D., Chauhan, M.S., 2014. Facile growth and characterization of α-Fe_2O_3 nanoparticles for photocatalytic degradation of methyl orange. J. Nanosci. Nanotech. 14, 1-5.
[29] Singh, R.N., Madhu, Abiasthi, R., Tiwari, S.K., 2009. Iron molybdates as electrocatalysts for O_2 evolution reaction in alkaline solutions. Int. J. Hydrogen Energy. 34, 4693-4700.
[30] Suresh, P., Prasada Rao, A.V., 2015. H_2O_2-assisted rapid visible light degradation of Carmine indigo, Crystal violet and Eosin Y with MoO_3 modified $Bi_2Mo_3O_{12}$. Asian J. Chem. 27, 2240-2244.
[31] Suresh, P., Umabala, A.M., Siva Rao, T., Prasada Rao, A.V., 2014. Visible light induced synergistic degradation of Rhodamine B, Methylene blue and Malachite green by $Fe_2(MoO_4)_3$ and MoO_3. J. Applic. Chem. 3, 696-701.
[32] Tian, S.H., Tu, Y.T., Chen, D.S., Chen, X., Xiong, Y., 2011. Degradation of acid orange II at neutral pH using Fe2(MoO4)3 as a heterogeneous fenton-like catalyst, Chem. Eng. J. 169, 31-37.
[33] Torkian, L., Amereh, E., 2012. Photocatalytic mineralization of Methylene blue aqueous solutions by Ag/TiO_2 nano composite. J. Appl. Chem. Res. 6, 16-23.
[34] Wu, D., Long, M., 2012. Visible light assisted photocatalytic degradation of methyl orange using Ag/N-TiO_2 photocatalysts. Water Sci. Technol. 65(6), 1027-1032.
[35] Yuan, H., Xu, J., 2010. Preparation, characterization and photocatalytic activity of nanometer SnO_2. Int. J. Chem. Eng. Applications, 1(3), 241-246.
[36] Zaleska, A., Doped-TiO2: A Review, 2008. Recent patents on Engineering. 2, 157-164.
[37] Zhang, D., 2013. Effectiveness of photodecomposition of rhodamine B and malachite green upon coupled tricomponent TiO_2 (Anatase-Rutile)/ZnO nanocomposite. Acta Chimica Slovaca. 6, 245-255.
[38] Zhao, X., Xu, T., Yao, W., Zhu, Y., 2009. Synthesis and photoelectrochemical properties of thin bismuth molybdates with various crystal phases. Thin solid films. 517, 5813-5818.
[39] Zhong, Jun bo, 2013. Photocatalytic decolourisation of methyl orange solution with phosphotungstic acid. Iran, J. Chem. Chem. Eng. 32, 57-65.
[40] Zhou, F., Zhu, Y., 2012. Significant photocatalytic enhancement in Methylene blue degradation of Bi_2WO_6 photocatalysts via graphene hybridization. Advanced Ceramics. 1, 72-78